EFDA–JET–PR(10)31

D. Testa, A. Fasoli, A. Goodyear, Q. King, P. Blanchard, H. Carfantan,
A. Klein, P. Lavanchy, T. Panis and JET EFDA contributors

The JET Alfvén Eigenmode Local Manager for the Real-Time Detection & Tracking of a Frequency-Degenerate Spectrum of MHD Instabilities

“This document is intended for publication in the open literature. It is made available on the understanding that it may not be further circulated and extracts or references may not be published prior to publication of the original when applicable, or without the consent of the Publications Officer, EFDA, Culham Science Centre, Abingdon, Oxon, OX14 3DB, UK.”

“Enquiries about Copyright and reproduction should be addressed to the Publications Officer, EFDA, Culham Science Centre, Abingdon, Oxon, OX14 3DB, UK.”

The contents of this preprint and all other JET EFDA Preprints and Conference Papers are available to view online free at www.iop.org/Jet. This site has full search facilities and e-mail alert options. The diagrams contained within the PDFs on this site are hyperlinked from the year 1996 onwards.

The JET Alfvén Eigenmode Local Manager for the Real-Time Detection & Tracking of a Frequency-Degenerate Spectrum of MHD Instabilities

D. Testa[1], A. Fasoli[1], A. Goodyear[2], Q. King[3], P. Blanchard[1,4], H. Carfantan[5], A. Klein[6], P. Lavanchy[1], T. Panis[1] and JET EFDA contributors*

JET-EFDA, Culham Science Centre, OX14 3DB, Abingdon, UK

[1]Ecole Polytechnique Fédérale de Lausanne (EPFL), Centre de Recherches en Physique des Plasmas, Association EURATOM – Confédération Suisse, CH–1015 Lausanne, Switzerland
[2]EURATOM-CCFE Fusion Association, Culham Science Centre, OX14 3DB, Abingdon, OXON, UK
[3]formerly: JET Joint Undertaking - Joint European Torus, Culham Science Centre, Abingdon, UK
[4]JET-EFDA Close Support Unit, Culham Science Center, Abingdon, UK
[5]Laboratoire d'Astrophysique de Toulouse – Tarbes, Université de Toulouse – CNRS, Toulouse, FR
[6]formerly: Plasma Science and Fusion Centre, Massachusetts Institute of Technology, Boston, USA
** See annex of F. Romanelli et al, "Overview of JET Results", (Proc. 22 nd IAEA Fusion Energy Conference, Geneva, Switzerland (2008)).*

Preprint of Paper to be submitted for publication in
Review of Scientific Instruments

ABSTRACT

We present the real-time VME system used to detect and track MHD instabilities, and particularly Alfvén Eigenmodes, on the JET tokamak. This system runs on a 1kHz clock cycle, and allows performing a real-time, unsupervised and blind detection, decomposition and tracking of the individual components in a frequency-degenerate, multi-harmonic spectrum, using a small number of input data which are un-evenly sampled in the spatial domain. This makes it possible to follow in real-time the detected modes as the plasma background evolves, and measure in real-time their frequency, amplitude, toroidal mode-number and damping rate. The successful implementation of this system opens a clear path towards developing real-time control tools for electro-magnetic instabilities in future fusion devices aimed at achieving a net energy gain, such as ITER.

1. INTRODUCTION.

The problem of blind and unsupervised real-time detection of the different components in a multi-harmonics spectrum using a small number of input data which are un-evenly sampled in the spatial domain is now becoming one of the main aspects required for machine protection and the control of plasma discharges in thermonuclear fusion experiments, and a wealth of literature is available on this subject (for some examples see Chapter3 and Chapter7 and references therein in Ref.[1] and Chapter2 and references therein in Ref.[2]). The method routinely used for this analysis involves sampling of a (relatively) small set of magnetic and non-magnetic signals, often containing some spatial periodicities so as to enhance or eliminate detection of certain components when the input signals are processed appropriately. A real-time algorithm then runs, and a global *alarm* is generated which may trigger a feedback control mechanism under certain specified conditions. The main drawback of this method is that it can only detect modes when they have become unstable, i.e. when they may have already had some, possibly detrimental, effect on the plasma background parameters. Conversely, an innovative method has been employed for quite some time now on the JET tokamak [3], which combines active excitation of magnetic field perturbations with a very small amplitude at the plasma edge (maximum intensity $\max(|\delta B_{DRIVEN}|)\sim 0.1G$, i.e. 10^5 times smaller than the typical value of the toroidal magnetic field in JET, $B_{TOR}\sim(1\text{-}3)T$) with synchronous real-time detection of the driven perturbations. This is the so-called Alfvén Eigenmodes (AEs) Active Diagnostic (AEAD) system [4, 5], of which the real-time Alfvén Eigenmodes Local Manager (AELM) constitutes one essential, moreover worldwide unique component. This diagnostic system allows the real-time detection and tracking of the driven modes, usually magneto-hydrodynamic (MHD) Eigenmodes supported by the plasma, when still stable, i.e. the modes have a positive damping $\gamma>0$, and have not yet caused any effect on the plasma background parameters. This is clearly a much more satisfying situation for machine protection and plasma control. The measurements of the mode frequency, damping rate, amplitude and toroidal mode number are passed to the JET Real Time Signal Server (RTSS), and their real-time estimate has been shown to be in very good agreement with the result obtained with a more detailed post-pulse analysis [6-8]. This allows in principle the

implementation of a control system and feedback for the modes, so that when the mode's damping rate reduces too much and approaches the marginal stability limit $\gamma/\omega = 0$, a control parameter (for instance the edge elongation in the case of AEs [6-9]) can be changed to bring the plasma back to a situation where it is further away from the marginal stability limit.

A recent upgrade of the AEAD system [10] to allow driving MHD modes with toroidal mode numbers (n) in the range $|n| \leq 30$, has shown conclusively that in this n-number range multiple AEs with different n's can be supported by the plasma at very close-by frequencies, such that the half-width at full-maximum of two modes (closely related to their damping and growth rate $\gamma/\omega = imag(w)/w$) is much smaller than their separation in frequency, practically leading to a frequency-degenerate spectrum. This has prompted the development and implementation within the AELM of a new real-time algorithm for the detection, discrimination and tracking of the individual components in such a frequency-degenerate spectrum, which is based on the method of *Sparse Representation of Signals* [11, 12].

This paper reports on the real-time development of the *Sparse Representation* method within the AELM hardware and software infrastructure, and on its specific application to the sub-millisecond detection, discrimination and tracking of the individual components in the multi-harmonic, frequency-degenerate spectrum of stable AEs which are excited in the JET tokamak by an array of external antennas used for MHD diagnostic purposes. This paper is organized as follows. In Section2 we briefly review the mathematical foundation of the *Sparse Representation* method (with a more complete overview given in Appendix-A). Section3 gives an overview of the AEAD system used in JET, with particular attention to its real-time plant control and data analysis hardware and software. Section4 then shows the first examples of the detection and discrimination between the different toroidal components in the multi-harmonic, stable spectrum driven by the AEAD system. Finally, in Section5 we briefly summarize our results and give an outlook towards future work.

2. THE SPARSE REPRESENTATION METHOD FOR THE REAL-TIME DETECTION AND DISCRIMINATION BETWEEN THE INDIVIDUAL COMPONENTS IN AN UNEVENLY SAMPLED, FREQUENCY-DEGENERATE, MULTI-HARMONIC SPECTRUM.

The problem of detection and discrimination between the individual components in a multi-harmonic spectrum which is un-evenly sampled in the spatial domain is common to various fields of physics and engineering [13]. Historically, this problem has been addressed using methods essentially based around the Lomb-Scargle periodograms [14-17], and much work has been done to improve on the limitations of these original methods, essentially in the field of Astronomy and Astrophysics (A&A). This general measurement problem is further complicated in thermonuclear fusion plasmas, and specifically in large-scale tokamak devices such as JET, by the very low number of measurement points in the spatial domain, due to in-vessel engineering and installation constraints, causing a number of mathematical difficulties. Therefore, analysis method based on the Nyquist criterion

cannot in general be used because of aliasing effect. This has prompted the developments and the applications of various methods to the analysis of MHD data in thermonuclear fusion plasmas, such as the Singular Value (SVD) [18, 19] and the wavelet [20] decomposition, the Wigner [21], Choi-Williams [22] and Hilbert [23] Transforms, and a generalization of the Lomb-Scargle periodograms [24]. However, none of these methods can be efficiently used for the decomposition of a frequency-degenerate, stable spectrum of MHD modes with the aim to measure their damping rate, because of their mathematical limitations and computational requirements, particularly when real-time, sub-millisecond calculations are needed.

Conversely, a method based on the *Sparse Representation of Signals*, as implemented in the *SparSpec* code (freeware available at: http://www.ast.obs-mip.fr/Softwares) has been demonstrated to perform efficiently and correctly the task of a post-pulse [25] and real-time [26] blind and unsupervised signal decomposition of unevenly sampled data using a very small number of measurement points. As some of the mathematical background of this method has been presented elsewhere [11, 12, 25, 26], here we only briefly review its theoretical foundations, with a more compete overview given in Appendix-A to facilitate the reading of this contribution.

In the standard tokamak coordinate system (toroidal angle ϕ, poloidal angle θ), and taking explicitly into account the usual 2D boundary conditions along the longitudinal (toroidal) axis and on the plane perpendicular to it (the poloidal direction), magnetic perturbations can be represented by functions involving toroidal (n) and poloidal (m) harmonics. Considering now the usual case of a perturbation with a specific toroidal mode number n, this can be written as $\psi(\omega,n)=e^{-i\omega t}e^{in\phi}\Sigma_m A_{mn}e^{imq}$, where each mode has one single toroidal mode number, but includes several poloidal harmonics. The aim of toroidal (poloidal) mode numbers detection is to measure the mode numbers n (m) of the magnetic instabilities present in the plasma and to estimate their amplitude from data acquired with P detectors unevenly positioned at angles ϕ_p (θ_p), $p=\{1,\ldots,P\}$. Hence each measurement y_p can be mathematically modeled as $y_p=\Sigma_l\alpha_l\exp(in_l\phi_p)+\varepsilon_p$, with $l=\{1,\ldots,L\}$, where n_l and α_l are the unknown mode numbers and amplitudes, respectively, L the unknown number of modes and ε_p corresponds to the noise on the data for the given p-th sensor. *Sparse Representations* solve the problem of determining the unknowns n_l and α_l by minimizing the L1-norm penalized criterion:

$$J_0(X)=\|y-Wx\|^2+\lambda\|x\|_1=\|y-Wx\|^2+\lambda\sum_{K=-K}^{K}(|X_k|). \qquad (1)$$

Here **y** is the vector of data taken at position ϕ_P; **x** is the vector of complex M=2K+1 components representing **y**, **W** is the spectral window, l is a penalization parameter related to the noise level, and the L1-norm is defined as the sum of the amplitudes of all the non-zero components in the measured spectrum. Many computationally efficient algorithms have been developed to solve eq.(1), and the *SparSpec* code uses one based on an iterative Block Coordinate Descent [11, 12] algorithm. A version of this algorithm has recently been adapted to perform the required mode decomposition analysis using the rather modest computational resources available to process real-time JET data [26].

3. THE ACTIVE MHD DIAGNOSTIC SYSTEM IN USE AT JET AND THE ALFVÉN EIGENMODE LOCAL MANAGER.

The *MHD spectroscopy* is a diagnostic technique that uses waves that are naturally supported by the plasma to measure the parameters that determine the dispersion relation, absorption and propagation, damping and growth of these waves [5, 27]. One example of such waves is Alfvén Eigenmodes (AEs): these modes are particularly important as they are a natural Eigenmode of any magnetically confined plasma, and because the fusion-produced αs are born with a supra-thermal speed that is typically super-Alfvénic in the usual thermonuclear tokamak plasma conditions. Therefore, resonant interaction with AEs is the first wave-particle interaction that the αs encounter during their thermalization: hence, this mechanism for phase-space and spatial diffusion needs to be controlled appropriately to guarantee good confinement of the αs themselves s [28, 29]. A simple active method to drive and detect low amplitude modes in the plasma was pioneered and used in many different plasma conditions in the JET tokamak [4]. This is the so-called Alfvén Eigenmodes Active Diagnostic (AEAD) system, and fig1 shows a very simplified schematic overview to illustrate its main features. The AEAD system principally consists of:

i) the AE exciter, built upon a function generator and a (high-power) amplifier connected to a set of in-vessel antennas (up to 8 in our case), whose aim is to send power into the plasma in order to drive a very small magnetic perturbation at the plasma edge, with maximum intensity max($|\delta B_{DRIVEN}|$)~0.1G, i.e. 10^5 times smaller than the typical value of the toroidal magnetic field in JET, B_{TOR}~(1-3)T;
ii) a receiver, built upon synchronous detection units, which is collecting signals from a set of in-vessel detectors for electro-magnetic fluctuations, such as magnetic pick-up coils, electron cyclotron emission and reflectometry measurements; this receiver is also connected to the real-time AE Local Manager (AELM) to allow for the detection and tracking of antenna-driven plasma resonances.

The AE exciter is built upon a 5kW class-B power amplifier capable of delivering up to a maximum I_{ANT}~10A-peak and a maximum V_{ANT}~1kV-peak in the frequency range 10kHz→500kHz to each of the 8 in-vessel antennas. The antennas are installed in two groups of four closely-spaced units located at two toroidally opposite positions but at the same poloidal location [10]. This allows the magnetic fluctuations to be driven with a sufficiently high $|dB_{DRIVEN}|>10^{-3}$G at the plasma edge for a spectrum of toroidal mode number extending up to $|n|$~30.

The plasma response to the antenna-driven perturbation is principally measured on a selected subset of signals using synchronous detection [4]. Looking at any electro-magnetic turbulence measurements, such as the signals from the magnetic pick-up coils, we would see that we measure a multitude of mixed frequencies. Conversely, for real-time use of the AEAD diagnostic, we need to measure only the plasma response at the frequency corresponding to the antenna excitation, i.e. the *synchronous* component. The purpose of the synchronous detection system is to select only the portion of the input signal which is at the same frequency as the one chosen for the excitation of

the modes: this also correspondingly reduces the required bandwidth of the data acquisition system (which has a 1.25kHz sampling rate for 12sec of each JET pulse, compared to the 1MHz sampling rate typical for the other JET fluctuation measurements), and also filters-out all other unwanted frequency components. The measured signal is then directly in relation (i.e. it is synchronous) to the launched antenna signal. The synchronous detection hardware works conceptually by applying a mixer with the synchronous in-phase (I) and quadrature (Q) components to the incoming differential signal, and then applying a low-pass filter with a <100Hz bandwidth to generate the output [cosine (I), sine (Q)] DC components. A schematic diagram of the synchronous detection hardware is shown in fig.2.

Synchronous detection is essential for the real-time applications (with plant protection and control using 24 channels, data analysis using 8 channels) to reduce the bandwidth required for data acquisition (a total of 48 channels in our case) and avoid the need for computationally expensive FFT-type algorithms. Post-pulse analysis can obviously still be performed using the much larger set of raw signals (between 32 and 80 additional channels depending on the operational setup) having the required sampling rate (at least 1MHz) via software-based synchronous detection. Further technical details on the active MHD diagnostic system used at JET can be found in [4, 7, 8, 10] and the references therein.

One essential and worldwide unique component of the AEAD system is the AELM. The AELM is a digital VME plant control system, used to monitor and control the operation of the AEAD plant in real time, with a 1kHz clock-rate. A schematic overview diagram for the AELM is shown in fig3. The AELM receives the feedback inputs for the AEAD system via ADC modules called VAJ1. These input data consist of 8 magnetic pick-up coils used for mode detection and 22 engineering signals (current and voltages measured at different point along the transmission line) used for plant control and normalization of the driven excitation spectrum. Additionally, two frequency deviation signals from the Ion Cyclotron Resonance Frequency (ICRF) antennas are also supplied as input to the AELM, and are used for RF beatwave control operation. The AELM is also supplied with the main plasma parameters via the RTSS, such as the plasma density, the magnetic field and the plasma current; these signals are required to compute in real-time the AE frequency. The AELM is also supplied with the overall JET timing signals originating from the Composite Time and Trigger Signal (CTTS) system. In addition to providing the timing control sequence for the AEAD system, the AELM produces a number of outputs sent back to the AEAD plant through DAC modules, again using the VAJ1 units. The main output is the AE frequency, called F_{REF}, which is a modulated DC voltage connected to the Voltage Controlled Oscillator (VCO) input of a function generator: the VCO frequency output is feedback controlled so that tracking can occur. The AELM also generates two other outputs but without feedback, which are sent to the AEAD control electronics. The first one consists of an amplitude waveform used as the reference current (I_{REF}) in an Active Gain Control (AGC) feedback amplifier loop. This waveform defines the target nominal antenna current that needs to be achieved during the discharge. The second output, which is also sent to the AGC, defines the maximum permissible voltage (V_{LIM}) allowed on the antennas, beyond which the AGC gain will

be reduced. Finally, the AELM produces the shorted-turn (S/T) signal for each individual antenna, and a global S/T trip alarm for protection of the plant. The S/T trip is generated in real-time via the AELM by computing the change of the antenna impedance, i.e. $d(V_{ANT}/I_{ANT})/dt = dZ_{ANT}/dt$: if this change is too sharp both in time and in its absolute value in any of the antennas, then a global S/T trip is generated to stop power being delivered to all the in-vessel antennas for at least 20ms, and as long as the alarm subsists, as this impedance change is suggestive of a short circuit between one (or more) of the antenna turn(s) and the vessel potential. These S/T trips have only occurred concurrently with Edge Localized Modes (ELMs) peeling off some portion of the edge plasma and dumping the associated current onto the wall, hence creating a very time- and space- localized short circuit between the plasma and the vessel potential, which is picked-up by the in-vessel antennas, and cause no real problem for the operation of the AEAD system. The AELM crate contains:

i) a VME Crate Service Module: this is a JET "home grown" module and acts as the VME system controller and provides timer and trigger synchronization with the plant systems; it also monitors the VME crate voltages, temperatures and airflow for operational control (plant failure);
ii) a Real-Time Processor (RtProc): this is an off-the-shelf Emerson Network Power MVME5500 card with a 1GHz PowerPC and 512MB RAM; this card executes software running under the Wind River VxWorks operating system, but during a JET pulse the main real-time process is "locked", so that context switching is disabled and most interrupt sources are masked;
iii) a Communications Processor (CommsProc): this is an off-the-shelf Emerson Network Power MVME5100 card with a 400MHz PowerPC and 64MB RAM. It is linked to both the JET real-time ATM and Ethernet networks and isolates the RtProc from asynchronous events that might disrupt its deterministic 1kHz calculation cycle time; the CommsProc also executes software running under VxWorks and is used to setup pre-pulse information, synchronize the RtProc with important time points within the pulse and finally communicates data recorded during the pulse for archiving;
iv) four off-the-shelf Pentland Systems MPV956 analogue and digital input/output cards (VAJ1): these cards are configured to use differential analogue inputs and sample 32 input signals (8 for mode detection, 24 for plant control); these cards are also used to send calculated analogue signals to control the power and frequency of the AEAD plant in real time.

The CommsProc can basically be thought of as a synchronization module that has four available states:

a) waiting for the next experiment to start: the CPU performs basic periodic environment and systems checks to ensure that all hardware and software are running correctly and the networks are able to send and receive "keep alive" data packets;

b) initialization for the next experiment: the CPU receives all the parameters for the experiment and configures the hardware and software accordingly;
c) pulsing/performing the experiment: the CPU synchronizes the sending and receiving of data over the real-time ATM network and triggers the RtProc based upon a 1kHz clock interrupt from the Crate Service Module; the CommsProc also ensures that the AEAD plant ceases to operate if there is either a CPU failure or an external systems failure that terminates the experiment prematurely;
d) data collection: the CPU halts the RtProc and returns all the data collected to the JET database archiving system for post-pulse analysis and simulation of plant operation.

The RtProc is only activated during an experiment (i.e. a JET pulse), otherwise it remains dormant. In its active state the RtProc operates on a 1kHz cycle, and the sequence of this cycle is as follows:

a) read and pre-process the analogue signals from the I/O cards (taking usually ~70μs);
b) perform the calculations required for S/T detection on the 8 antennas, so that if a faster-than-normal change in the antenna impedance is identified, then the AELM will send a trip signal to the amplifier to suspend its output for 20ms for plant protection (these calculations take usually ~50μs); the user is able to configure the total number of trips tolerated before one (or more) antenna(s) is (are) permanently excluded from the remainder of the pulse;
c) perform mode detection, discrimination and tracking using one of two user-selectable options, described below in more details: the calculations performed in the "SimpleSum" mode take usually ~100μs, whereas those required for the "SparSpec" mode take usually ~650μs;
d) finally, the VCO frequency is calculated and sent back to the AEAD plant for the next time step, together with the requested IREF value (taking usually ~50μs).

The selection of the run-time parameters for the operation of the AEAD system is performed via a configuration panel, and fig4 shows its main operating window for the SparSpec algorithm when the real-time value of the TAE frequency is used for frequency control. There are two possibilities for selecting the frequency source FREF: a pre-defined waveform (mostly used for commissioning and testing purposes) and an algorithm to evaluate the real-time AE frequency, based on the measurement of the magnetic field, plasma current and density (the usual selection, labeled "AELM"). As shown in fig6, the choice is made by selecting the "Fref Source" tab on the AELM configuration panel; on top of any of these one can also select the RF beatwave control mode via the "RF Fdev" tab (this option is however very rarely used as it requires the AELM to take control of two out of the four RF generators). Finally, if using the RTSS and AELM mode selected for the FREF source, a low-pass, 50Hz filter can then be applied to the FREF value so as to smooth-out any spikes coming from the input plasma data. The maximum operating frequency for the AEAD plant is set by the corresponding tab (500kHz in the case shown in fig4). If the "AELM" mode is selected for the FREF source, then, as shown in fig6, a number of additional parameters need to be set according to the formula

F_{REF}[kHz]=32.7x[F_{REF}Multiplier×Itf[A]/sqrt(MassNumber×Density[$10^{18}m^{-2}$])]×(Ip[A]/IpNorm[A])

The required parameters for the "AELM mode" are defined as follows, giving F_{REF} in units of kHz:

parameter	**source**	**explaination of use**
density	RTSS input (real-time data)	line-averaged plasma density (units:[1018m-2])
ltf	RTSS input (real-time data)	current in the torodial field coils (units:[A])
lp	RTSS input (real-time data)	toroidal plasma current (units:[A])
Mass Number	user selection: can take any value >0	chosen according to the main plasma gas: • MassNumber=1 for H-plasmas • MassNumber=2 for D and He4-plasmas
F_{REF} Multiplier	user selection: can take any value >0	chosen to change the nominal F_{REF} frequency by a constant multiplicative factor; • F_{REF} Multiplier=1 for the TAE range • F_{REF} Multiplier=2 for the EAE range
ipNorm	user selection: can take any value ≥ IpNorm	normalisation plasma current (units:[A]) usually chosen as the nominal flat-top value of the plasma current (IpNorm=2.5e6[=2.5MA] in fig 6)
	not intended to be used	

Once the choice of the frequency source has been made, the *scanning* or *tracking* mode may be selected. If frequency scanning is disabled, the AELM will output exactly the frequency set using the F_{REF}, i.e. the antenna frequency F_{ANT} is in the range $0 \leq F_{ANT} = F_{REF} \leq F_{MAX}$. When the *scanning* mode is *enabled*, a pre-defined up/down symmetric (repetitive) sweep, with parameters setup via the AELM, is added to the chosen F_{REF}. The values for the scan half-width (kHz) and speed (kHz/sec) can be selected separately for the limiter and X-point ("diverter") magnetic configurations. The permissible values are "*ScanWidth*" = (0à400)kHz and "*ScanSpeed*" = (0→400)kHz/sec in both configurations, the usual values for operation being "*ScanWidth*" = (100→250)kHz and "*ScanSpeed*" = (100→250)kHz/sec. When the *tracking* mode is *enabled* (which can only be used if *scanning* is enabled), the real-time mode detection algorithm is used to lock the AELM frequency scan around the frequency of the detected modes, so as to track their evolution in real-time. This is done by reversing the direction of the frequency sweep when certain resonance conditions are met (see below for further details), or at the extrema of the frequency scan F_{REF} ± ScanWidth when these conditions are not met.

The V_{LIM} control is set using the tab "*SC voltage limit*": the maximum voltage allowed on the antennas is $V_{LIM} = \max(V_{ANT}) = 700$V-peak, and the usual value chosen for operation is $V_{LIM} =$ 600V-peak. The I_{REF} control is set using the tab "*InputPowerSelector*", which can be either a fixed-level value or a time-dependent waveform. The maximum allowable current I_{REF} (corresponding to a power = 100% setting in the AELM) is $I_{REF} = \max(I_{ANT}) = 15$A-peak on the antennas. Various

parameters need to be set for the algorithm producing the S/T trip: the allowable low-pass filter frequency for all the I_{ANT} and V_{ANT} data, and for the processed Z_{ANT} and STant=dZ_{ANT}/dt data are all in the range 0.1à400[Hz], the usual values for operation being 100Hz for the three filters. The usual value for the S/T trip threshold, defined in the "*STantThreshold*" tab, is 100[W/sec], and the usual value for the maximum number of allowed S/T trips during one single discharge, defined in the "*STantMaxTrips*" tab, is =100.

To detect and track in real-time the individual resonances corresponding to antenna-driven, stable plasma modes, the AELM linearly sweeps the antenna frequency around an initial guess for the mode's resonance. One of two algorithms can be selected to derive a single amplitude and phase pair that will be used for mode detection and tracking: the original (~10 years old) "*SimpleSum*" algorithm combines up to 8 real and imaginary pairs from the total 8 input data available to obtain one single pair of real and imaginary components, whereas the newly developed "*SparSpec*" algorithm can also accept up to 8 input real and imaginary pairs but produces many output amplitude and phase pairs. When using the *SparSpec* tracking mode, the AELM has two methods, "*highest*" and "*any*", for selecting the pair to use for tracking: the *highest* method picks the pair with the greatest amplitude, whereas the *any* method looks for a pair where the amplitude is above a given threshold; if a resonance is detected, this pair will continue to be selected until tracking is lost when the search for a new pair will commence. When the AE resonance is met, the exciter frequency is swept back and forth around it. A Lorentzian model fit of the antenna/plasma transfer function is used to obtain the mode frequency and quality factor in real-time, and the mode amplitude at the different probes. This simple real time estimate of the mode frequency and damping rate from the centre and width of the driven resonance follows very closely the value obtained from a post-pulse analysis [6-8].

Figure5 shows an illustrative example of the AEAD plant in the tracking mode of operation. In the full-frequency spectrum (shown in the left frame) we see a triangular waveform that sometimes becomes very narrow in an otherwise completely clean portion of the fluctuation spectrum: this is the antenna frequency, which was set to look for resonances around the frequency of an n = 3 Toroidal Alfvén Eigenmode (TAE) as evaluated in real-time for that shot (i.e. around 200kHz). In the right frame, we have the synchronous detected signal ($|\delta B_{MEAS}|$) from one magnetic pick-up coil, showing the real-time TAE frequency (f_{TAE}) and the antenna frequency. Narrow sweeps of the antenna frequency occur when the complex-valued dB_{MEAS} (shown in the two inserts) is sufficiently close to the pre-set resonant shape, i.e. it describes a circle in the complex plan representation with a corresponding bell-shape in the $|\delta B_{MEAS}(\omega)|$ representation. We are then *tracking* the mode, and its frequency (f_{MEAS}) and damping (γ_{MEAS}) are measured in real-time. Such narrow sweeps occur between t = 8→10sec and t = 11→14sec. The much larger frequency sweeps indicate that no resonance close to the pre-set value has been detected in real-time: we are then *scanning* for a mode, and the AELM looks for antenna-driven plasma resonances in a different frequency range. This approach allows the detection and tracking of hundreds of individual resonances during one single tokamak discharge, which are guaranteed to be the same mode, i.e. to have the same *n*-number, if

the *SparSpec* algorithm has been used.

As shown in fig4, the AELM configuration panel has many tabs requiring user input for the mode detection algorithm, which is selected via the tab "*DetectorSignal*"; the parameters which are common to the *SimpleSum* and *SparSpec* algorithms are as follows:

polarity	defines the signal polarity (+ve or -ve) associated to the selected sensor
filter	cut-off frequency for a real-time low-pass filter applied to all the raw data
thresholds	define the amplitude ($d\|\delta B_{MEAS}\|/dt$) and speed ($d(\|\delta B_{MEAS}\|)/dI_{ANT}$) at the start/end of a frequency scan to recognize if a plasma resonance is indeed associated to a mode of sufficiently high amplitude ($d\|\delta B_{MEAS}\|/dt$>AmpThresh) and sufficiently close to marginal the stability limit $\gamma/\omega=0$ ($d(\|\delta B_{MEAS}\|)/dI_{ANT}$>SpeedThresh) to be of interest for real-time detection and tracking (see also the illustrative sketch shown in fig6)
Minimum Twist	defines the minimum angle threshold $d(imag(\delta B_{MEAS}))/d(real(\delta B_{MEAS}))$ in the complex plane representation to recognize if a mode detected using the amplitude and speed thresholds defined above is antenna-driven and stable ($\gamma/\omega>0$) (see also fig6)
Normalising Detector	used in tracking mode to normalize the measured: this can be anyone of the antenna currents or voltage, or it can be set to "off" (i.e. no normalization is used)
Cdamp Constant	defines the constant conversion factor for the real-time calculation of the damping rate as estimated from the frequency width of the detected resonance (see [6])

Figure6 shows graphically an intuitive description of the usage of these parameters. At the beginning of each frequency scan, if a mode has been detected (via the *SimpleSum* or the *SparSpec* methods), we check that its amplitude ($d|\delta B_{MEAS}|/dt$) and speed ($d(|\delta B_{MEAS}|)/dI_{ANT}$) are above the set thresholds (bottom left plot: AmpThresh = 0.65×10^{-9}[T/s] and SpeedThreshStart = 5×10^{-13}[T/A]); if these conditions are satisfied, we start computing the time-integrated twist (bottom right plot) using the complex plane representation of $\delta B_{MEAS}(\omega)$ (top plot); we estimate that the antenna-driven plasma resonance has been fully identified when the integrated twist value exceeds the set threshold $=2p$ and if the speed is below the set SpeedThreshEnd $=6\times10^{-13}$[T/A]; hence the direction of the frequency sweep is reversed (as shown in the insert in the top plot) in an attempt to follow the evolution of the same mode as the background plasma evolves.

When the *SimpleSum* algorithm is selected, the following parameters also need to be set (see fig7a):

Number	fixed: defines the eight input channels (TAE-SIG/01-08)
Multiplier	multiplicative factors (used=0) used to combine the eight input TAE-SIG/01-08 and generate one single output, allowing a discrimination between n=odd and n=even modes when pairs of sensors located at toroidal opposite positions are subtracted or summed

When the *SparSpec* algorithm is selected, the following parameters also need to be set (see also fig7b):

Mode	defines the option used for selecting which n-number mode has to be tracked in real-time (highest or any)
AmpCalc	defines the option used for computing the absolute amplitude of the mode via a LS estimation (yes or no)
N-selection	defines the n-numbers $\lvert n\rvert \leq N_{MAX}$ that need to be detected and discriminated; since the SparSpec algorithm defaults to the N_{MAX} if no mode is found within the allocated CPU time, the value $\lvert n\rvert = N_{MAX}$ is kept so as to easily see when no mode has been found in real-time, as we set for N_{MAX} a mode not usually present in the plasma
sensor	defines which sensor is associated to that particular channel (can be "unused")
T-entry	defines the angular position of the sensor associated to that particular channel
SS-nmax	defines the maximum n-number to be included in the calculation of the sparse spectrum; this value must be larger than N_{MAX}
SS-threshold	defines the background noise level threshold in the $\lvert\delta B_{MEAS}\rvert$ spectrum
SS-lambda	if the SparSpec algorithm has been selected, defines the λ_{NORM}-parameter

4. REAL-TIME, BLIND, UNSUPERVISED DETECTION AND DISCRIMINATION OF DIFFERENT TOROIDAL COMPONENTS IN A FREQUENCY-DEGENERATED SPECTRUM OF MHD INSTABILITIES USING THE AELM.

One of the first results obtained with the AEAD diagnostic system in the most recent JET experimental campaigns has been that, despite the very low magnetic field driven by the antennas for medium-n AEs (in the plasma core we have $\lvert\delta B_{DRIVEN}\rvert \sim 1\times10^{-3}$G for n = 5 compared to $\lvert dB_{DRIVEN}\rvert \sim 5\times10^{-2}$G for the n = 1 and n = 2 modes), many modes with $\lvert n\rvert \sim 0$-12 and very low-damping rate $\gamma/\omega < 0.2\%$ were found to be simultaneously excited in plasmas without populations of resonant fast ions [7, 8]. Correct real-time detection and n-number discrimination of these modes is particularly important as their low intrinsic (i.e. without any fast ion drive) damping rate makes them very prone to become unstable if resonant fast ions were present in the plasma. It is specifically this experimental observation that has prompted the development of the more sophisticated real-time algorithm for mode-number recognition based on the *SparSpec* algorithm, which has now almost completely replaced the original *SimpleSum* method.

The capability to perform a blind and unsupervised real-time detection and tracking of the individual n-components in the antenna driven spectrum constitutes an invaluable tool, which is unique to the JET tokamak. It provides accurate testing for the code prediction for the damping rate of Alfvén Eigenmodes (see for instance the results presented in [9]), as it is paramount that the same mode be measured throughout the parameter scan. The full implementation of the *SparSpec* algorithm in the AELM software now allows a detailed quantitative analysis of the recent measurements made with the AEAD system in JET. Mode numbers can be directly separated in real-time and individually tracked to measure the changes in the mode frequency and g/w during the evolution of the plasma background. It is also paramount that the real-time detection matches

the results obtained via the more complex and accurate post-pulse analysis method, and this has been discussed and demonstrated in detail in [7, 8].

Figure 8a shows an example of the real-time detection and tracking of individual n = 3, n = 5 and n = 7 TAEs for the JET Pulse No: 77417, where the excitation system was configured to drive predominantly n-odd modes, with $\max(|\delta B_{DRIVEN}(n)|)$ in the range $|n|<5$. For this shot, the AELM tracking algorithm was configured in the "*SparSpec-highest*" mode, with Amp.Thresh = 3×10^{-9}T/s, Speed.Thresh = 3×10^{-13}T/A, Minimum.Twist = 2rad, $\lambda_{NORM} = 0.9$, $N_{MAX} = 10$ and detection for modes with n = 3-10(i.e. only co-current propagating). The digital signals shown at the bottom of fig10a indicate whether detection and tracking of a certain mode has been successful: if the validity flag is set to high=1 then the corresponding mode has been correctly detected and tracking is occurring, otherwise the digital signal is set to low = 0 (note that it is in principle possible to have a valid $n=N_{MAX}$ mode as long as the validity flag is = 1: therefore, it is the validity flag that denotes "good" or "bad" tracking for the $n = N_{MAX}$ mode). At the start of each real-time scan, the *mode* value was initialized to a *bad* value of $n = N_{MAX}$ and its associated digital validity flag set to 0 (not shown in fig8, where we only show the digital flags for certain specific n's to reduce cluttering). In fig8a we note that the antenna frequency waveform F_{TAE} follows closely the real-time evolution of the reference TAE frequency F_{REF}, and that the n = 3 mode is the one most detected in real-time. This is consistent with the fact that (a) the excitation spectrum was larger for $|n|<5$, and that (b) counter-current propagating modes ($n<0$) and modes with $n<3$ were not selected for real-time detection via the AELM. These results are confirmed by a more detailed post-pulse analysis using the full implementation of the *SparSpec* algorithm, which includes detection and discrimination between all modes up to $|n| = 30$, using $\lambda_{NORM} = 0.7$ to help in resolving also lower-amplitudes modes. This analysis is shown in fig8b, where we plot the mode frequency and damping rate γ/ω as sorted for decreasing mode amplitude for all the detected TAEs, but only few values for the normalized excitation spectrum $|\delta B(n)/\mathrm{sum}(I_{ANT})|$ to reduce cluttering.

To illustrate in more details the logic of the *SparSpec* tracking algorithm as implemented in real-time in the AELM, fig.9 shows an example of the real-time time twist and speed calculations for the n = 11 TAE mode in the JET Pulse No: 77790, where the excitation system was configured to drive predominantly n-odd modes, with $\max(|\delta B_{DRIVEN}(n)|)$ in the range $|n|\sim5$-10. For this shot, we used the tracking mode *SparSpec-highest*, with $N_{MAX} = 15$, $\lambda_{NORM} = 0.95$, Amp.Thresh = 1×10^{-9}T/s, Speed.Thresh = 3×10^{-13}T/A, Minimum.Twist = 2.5rad, and detection for modes with n = [−15, −11, −9, −7, −5, 5−11]. Comparing in fig.9a the status of the digital flags for the amplitude (SigAmp.11) and speed (Speed.11) for the n = 11 mode, we note that it is only when these two signals are concurrently high that the corresponding digital flag for the differential twist (TwistRate.11) is also set to high, hence the integrated twist is being calculated and tracking of the n = 11 mode can occur (mode signal set to = 11) if the integrated twist exceeds the set threshold. Specifically, this mostly happens in the time window 5.0<time(sec)<9.5 (an highlight of this is shown in fig9.b), rarely in other time intervals, indicating a subtle dependence of the stability of the n = 11 mode as

function of the background plasma parameters.

Finally, when combining the real-time mode number, frequency and damping rate data obtained in various shots (hence with different plasma configurations and background parameters) when different setups were used for the *SparSpec* tracking algorithm within the AELM (such as different values for N_{MAX}, Amp.Thresh, Speed.Thresh, Minimum.Twist, and the n's selected for real-time detection), and using different excitation spectra, we can compare these data with the corresponding ones obtained with the post-pulse analysis. This allows us to obtain a statistical analysis of the accuracy of the real time measurements. For this, we consider the expectation value on the mode number, frequency and damping rate as the one given by the post-pulse analysis, use the actual post-pulse estimation on the errors on these quantities, which are typically around the values presented in [7] (i.e. ~10% on the n's and frequency, ~25% on γ/ω) and define a *confidence level* for the real-time measurements as:

$$\text{confidence level} = \exp\left(\frac{(\text{RealTimeData - PostPulseData})^2}{(\text{VariancePostPulseData})^2}\right) \tag{2}$$

The Gaussian *confidence level* data obtained with this procedure are shown in fig.10 as function of the toroidal mode number for all the modes for which we have sufficient statistics. We note that the confidence level is quite high for all the real-time data obtained with the *SparSpec* tracking algorithm, at least exceeding 0.8 for all mode numbers in the range $-8<n<12$. This proves that the *SparSpec* real-time mode detection and tracking algorithm can indeed be used as a valuable diagnostic tool for blind and unsupervised mode discrimination in a multi-components and frequency-degenerate spectrum.

SUMMARY AND CONCLUSIONS

In this work we have reported on the application of a new method for the real-time and unsupervised detection and decomposition of a multi-harmonic and degenerate spectrum of high-frequency magnetic instabilities measured on the JET tokamak, i.e. one where the frequency separation between the various components is less than their half-width at full-maximum. This method uses real-time measurements performed on a 1ms time base, processed by the AELM, which is a VME system interfacing with the JET RTSS system. The real-time mode detection and discrimination algorithm is based on the Sparse Representation of signals, derived from its original applications to astronomical data via the *SparSpec* code. The development of this method was prompted by the first measurements in the JET tokamak of such a frequency degenerated spectrum of antenna-driven AEs, with toroidal mode numbers $|n|\sim3$-15. The real-time (and post-pulse) implementation of the *SparSpec* algorithm on JET has allowed a complete, accurate and numerically efficient analysis of these measurements, which would have not been possible otherwise. For post-pulse analysis, the antenna-driven spectrum can be decomposed and analyzed for one whole frequency scan typically within (2-3)μs of CPU time using the full (more complex and more accurate) implementation of the *SparSpec* algorithm. With an SVD decomposition algorithm similar to the one presented in [19], requiring a combinatorial exploration of all possible solutions and an a-posteriori thresholding scheme to determine the correct ones, or using wavelet-based schemes, such as those presented in [20], this analysis would require a CPU time

usually in excess of 150ms for each individual frequency scan. Such computational requirements make it impossible to use these schemes for real-time analysis. Conversely, using the rather modest computational resources allocated to the real-time analysis of the AEAD data within the AELM hardware and software (a 1GHz PowerPC with a 512MB RAM running on a 1kHz clock-rate), the multi-components antenna-driven spectrum can be fully resolved within typically ~650μs for each 1ms clock-cycle. Finally, the results for the mode frequency, damping rate, mode numbers (and scaled mode amplitude) obtained with the real-time *SparSpec* algorithm are in good agreement both statistically and on a shot-by-shot basis with those obtained with the post-pulse implementation of this algorithm, confirming that the AELM system can indeed be valuably used for real-time analysis for plasma control purposes.

For JET, and more generally fusion plasmas, further applications of this new method based on the *Sparse Representation of Signals* open interesting and very useful perspectives for the concurrent real-time detection and control of different MHD instabilities, as they can be discriminated very accurately. This allows specifically tailored control schemes to be put in place for each individual mode, hence improving the overall control of the plasma operation and performance. This will be particularly important for future experiments approaching the burning plasma conditions, such as ITER, where real-time control of the stability of the fusion born alphas in the background "sea" of MHD modes that are expected to occur in such conditions, represents one of the key ingredients required to achieve a net fusion energy gain. Furthermore, and while specifically applied for the analysis of astronomical data and toroidal mode numbers in thermonuclear fusion plasmas in a tokamak device, the use of *Sparse Approximations* methods are ideally suited for applications to all domains of data analysis, control engineering and system design where an efficient decomposition of a multi-harmonics degenerate spectrum is required from irregularly sampled data. An example of this work is the application of the *SparSpec* algorithm to the analysis and optimization of the baseline design for the diagnostic system intended for the measurement of high-frequency instabilities in ITER [30].

ACKNOWLEDGEMENTS.

This work, supported by the European Communities under the contract of Association between EURATOM and CRPP-EPFL, was carried out within the framework of the European Fusion Development Agreement. This work was also partly supported by the Swiss National Science Foundation. The views and opinions expressed herein do not necessarily reflect those of the European Commission. The Authors would like to thank the various members, past and present, of the CRPP, MIT and JET staff that have contributed to the design, installation, commissioning and operation of the Alfvén Eigenmode Active Diagnostic system over more than 10 years of experimental runs at JET.

REFERENCES

[1]. Various Authors, "Progress in the ITER Physics Basis", Special Issue of Nuclear Fusion **47** (2007).

[2]. E.J. Strait, E.D. Fredrickson, J-M. Moret, M. Takechi, Fusion Science Technology 53 (2) (2008), 304.
[3]. J. Wesson, Tokamaks, 3rd edition, (Oxford Science Publication, Oxford, 2003), p.617.
[4]. A. Fasoli et al., Physical Review Letters **75** (1995), 645.
[5]. A. Fasoli, D. Testa et al., Plasma Physics and Controlled Fusion **44** (2002), 159.
[6]. D. Testa and A. Fasoli, Nuclear Fusion **41** (2001), 809.
[7]. D. Testa et al., Nuclear Fusion **50** (2010), 084010.
[8]. T. Panis, D. Testa et al., Nuclear Fusion **50** (2010), 084019.
[9]. The ITPA working group, to be presented at the IAEA Fusion Energy Conference 2010.
[10]. D.T esta et al., The new Alfvén Wave Active Excitation System at JET, Proceedings 23rd SOFT Conference 2004 (weblink: http://infoscience.epfl.ch/record/143354/files/).
[11]. S. Bourguignon, H. Carfantan, T. Böhm, Astronomy and Astrophysics **462** (2007), 379.
[12]. S. Bourguignon, H. Carfantan, J. Idier, IEEE Journal of Selected Topics in Signal Processing **1** (2007), 4.
[13]. F. Marvasti, Non-Uniform Sampling: Theory and Practice, Springer-Verlag (2001).
[14]. N.R. Lomb, Astrophysics and Space Science **39** (1976), 447.
[15]. J.D. Scargle, The Astronomical Journal **263** (1982), 835.
[16]. D. Roberts, J. Lehar and J. Dreher, The Astronomical Journal **93** (1987), 968.
[17]. G.Foster, The Astronomical Journal **109** (1995), 1889.
[18]. J.S.Kim et al., Plasma Physics and Controlled Fusion **41** (1999), 1399.
[19]. M. Hole and L. Appel, Plasma Physics and Controlled Fusion **49** (2007), 1971.
[20]. F.M. Poli et al., Plasma Physics and Controlled Fusion **50** (2008), 095009.
[21]. E.P. Wigner, Physics Review **40** (1932), 749.
[22]. H. Choi, W. Williams, IEEE Trans. Acoust. Speech Signal Process **37** (1989), 86.
[23]. N.E. Huang et al., Proc. Royal Society London A**454** (1998), 903.
[24]. S. Zegenhagen, A. Werner et al., Plasma Physics and Controlled Fusion **48** (2006), 1333.
[25]. A. Klein, H. Carfantan, D. Testa, et al., Plasma Physics and Controlled Fusion **50** (2008), 125005.
[26]. D. Testa et al., An algorithm for the real-time and unsupervised detection, decomposition and tracking of the individual components in a degenerate, multi-harmonics spectrum, submitted for publication to EuroPhysics Letters, June 2010.
[27]. S. Sharapov, D. Testa et al., Physics Letters A **289** (2001), 127.
[28]. W.W. Heidbrink, Physics of Plasmas **9**(5) (2002), 2113.
[29]. G. Vlad, S. Briguglio, G. Fogaccia, F. Zonca, Nuclear Fusion **46** (2006), 1.
[30]. D. Testa et al., Fusion Science Technolgy **57**(3) (2010), 208-237.
[31]. J. Lafler and T.D. Kinman, The Astrophys Journal Supplement **11** (1965), 216.
[32]. M.M. Dworetsky, Mon. Not. R. Astron. Soc. **203** (1983), 917.
[33]. P.Stoica, R.L. Moses, B.Friedlander, and T.Söderström, IEEE Trans. ASSP **37** (1989), 378.
[34]. J.-J. Fuchs, IEEE Transactions on Information Theory **51** (2005), 3601.

[35]. D.L. Donoho, M. Elad, and V.N. Temlyakov, IEEE Transactions on Information Theory **52** (2006), 6.
[36]. J.A.Tropp, IEEE Transactions on Information Theory **52** (2006), 1030.
[37]. D.Donoho, Journal of Communications on Pure & Applied Mathematics **59** (2006), 797.
[38]. D.M.Malioutov, A sparse signal reconstruction perspective for source localization with sensor arrays, Master Thesis, MIT, July 2003.
[39]. J.A.Tropp, IEEE Transactions on Information Theory **50** (2004), 2231-2242.

APPENDIX-A: SPARSE REPRESENTATIONS AND THE SPARSPEC CODE.

In the standard tokamak coordinate system (toroidal angle f, poloidal angle θ), and taking explicitly into account 2D boundary conditions along the longitudinal (toroidal) axis and on the plane perpendicular to it (the poloidal direction), magnetic perturbations can be represented by functions involving toroidal (n) and poloidal (m) harmonics. Considering now the usual case of a perturbation with a specific toroidal mode number n, this can be written as $y(w,n)=e^{-i\omega t}e^{in\phi}\Sigma_m A_{mn}e^{imq}$, where each mode has one single toroidal mode number, but includes several poloidal Fourier harmonics. The aim of toroidal (poloidal) mode numbers detection is to detect the mode numbers n (m) of the magnetic instabilities actually present in the plasma and to estimate their amplitude from data acquired with detectors unevenly positioned at angles ϕ_p (θ_p) in radians, $p=\{1,\ldots,P\}$ being the suffix labeling the individual sensors used for the measurement. Mathematically, each measurement y_p is modeled as:

$$y_p=\sum_{l=1}^{L}\alpha_l e^{inl\phi_p}+\varepsilon_p \qquad \text{A1}$$

where n_l and α_l are the unknown mode numbers and amplitudes, respectively, L the unknown number of modes and ε_p corresponds to the noise on the data for the given p-th sensor. This problem, which amounts to fitting multiple cissoids to the input data, is a very general signal processing problem which arises in many fields of physics. However, it is particularly difficult in the case of tokamak plasma physics as the data is unevenly sampled and sparse, because of unavoidable installation constraints on the measurement devices. Such a spectral analysis problem from irregularly sampled data is very common in A&A, where time series acquisition usually suffer from incomplete temporal coverage, in particular periodic gaps caused by the Earth's rotation and revolution, and a-periodic interruptions due to the weather. Many methods have been proposed in the fields of A&A to improve the analysis of such irregularly sampled time series, based on generalizations of the Lomb-Scargle periodogram [14, 15] and Date-Compensated Discrete Fourier Transform [31]. These methods involve iterative analysis [17], generally used when dealing with a large number of data points, or

fitting periodic signals (Phase Dispersion Minimization [32], string length method [33]) to short data strings. Such methods, however, are inadequate when there are several temporal frequencies and too few measurement points.

The mathematical problem described by eq.(A1) can be expressed equivalently in the Fourier spatial domain (i.e. using a Fourier transform with respect to the angular position ϕ) as:

$$\hat{y}(\nu)=\sum_{P=1}^{P} y_p e^{i\nu\phi p}=\hat{W}(\nu)*\sum_{l=1}^{L}\alpha_1\delta(\nu-n_l)+\hat{\varepsilon}(\nu) \qquad \text{A2}$$

where δ is the Dirac delta function, the "^" symbol indicates the Fourier transform of the data ($\hat{y}(\nu)$ and noise ($\hat{\varepsilon}(\nu)$ samples, the symbol "$*$" is the convolution operator and ($\hat{W}(\nu)$ is the spectral window of the sampling scheme. It can be shown that the difficulty of the spectral analysis problem is closely related to properties of the spectral window, such as the height of secondary lobes. In A&A, when accounting for long times series, high secondary lobes are due to periodicities, typically daily, of the temporal gaps in the measurement (see figA1, top frame), while in thermonuclear tokamak plasmas these lobes are due to regularities in the sampling (for instance when using a spacing larger than the Nyquist condition) and to the low number of sensors (see figA1, bottom).
When applied to thermonuclear plasma physics, the problem has some additional specificity. First, the data are complex-valued, implying that the Fourier transform of the data does not satisfy the Hermitian property $\hat{y}(-\nu) = \hat{y}^*(\nu)$ as in the spectral analysis of real-valued data. Second, the modes numbers n_l can only take positive or negative integer values, while in the general spectral analysis problem frequencies take real values. Third, in the real time applications we consider for JET, a set of data is acquired every 1ms, therefore the spectral analysis must be completed in an unsupervised manner in the short time between each measurement acquisition.

Evaluating the amplitudes α_l and the modes number n_l of multiple modes in a multi-harmonic spectrum is a very difficult problem, even if the number of modes in the input spectrum is actually known a-priori. The usual way to tackle this problem is performing a best Least-Square (LS) fitting of the input data. However, this criterion has many local minima for real valued spectral peaks [34-36], hence in principle requiring a combinatorial exploration for integer-valued mode numbers n_l, and an a-posteriori thresholding scheme to differentiate the "correct" from the "wrong" solutions, which is very much CPU-time consuming and cannot possibly be adapted for real-time applications on the sub-millisecond time scale required for the analysis of the JET measurements. The only possibility to solve this problem is to provide an estimate for the amplitudes of all possible modes numbers in the range $\{-K, \ldots, K\}$ (where $|K|$ is much larger than the maximum mode number that can be conceivably present in the input spectrum), at the same time enforcing that most of these modes actually have a null amplitude, i.e. a utilizing a *Sparse Approximation*.

Formally, *Sparse Representations* [12, 37, 38] are representations that account for all information in the input data with a linear combination of a small number of elementary signals called *atoms*. The atoms set does not form a basis as the number of atoms exceeds the dimension of the signal

space, so any signal can be represented by more than one combination of different atoms. Among all these various possible combinations, the one with the smallest number of atoms is the Sparse Representation of the signal. The Sparse Approximations of signals is the version of the Sparse Representations adapted to noisy data. Theoretically, the Sparse Approximation problem consists of minimizing the criterion:

$$J_0(X) = \| y - Wx \|^2 + \gamma \|x\|_0. \qquad \text{A3a}$$

Here $\mathbf{y}=[y_1, y_2, \ldots, y_P]^T$ is the vector of data taken at position ϕ_P; $\mathbf{x}=[x_1, x_2, \ldots, x_M]^T$ is the vector of complex amplitudes, $\mathbf{W}=[\mathbf{w}_1, \mathbf{w}_2, \ldots, \mathbf{w}_M]$ is a matrix where the vector $\mathbf{w}_k$ corresponds to the k-th atom, the L0-norm of $\mathbf{x}$: $\|\mathbf{x}\|_0 = \#\{k, |x_k| \neq 0\}$ is the number of non-zero components of $\mathbf{x}$ and g is a penalization parameter. However, to minimize this criterion, one must sift through all possible combinations of elementary signals, which is intractable for large M. Hence, two kinds of methods have been proposed to get round this problem. The first one, often called *greedy pursuit* algorithms, iteratively adds atoms to the approximation of the signal to improve this approximation [39]. The second one, often called *convex relaxation*, replace the L0-norm in criterion (A3a) with another penalization term such that the criterion may be minimized more easily. In our work, we follow this convex relaxation approach, using the classically used L1-norm (see for instance [12, 37, 38]) as it leads to the criterion:

$$J_0(X) = \| y - Wx \|^2 + \lambda \|x\|_1 = \|y - Wx\|^2 + \lambda \sum_{K=-K}^{K} (|X_k|). \qquad \text{A3b}$$

It can then be easily shown that the criterion of eq.(A3b) is convex, therefore has no local minima, but, as the number of unknowns may be larger than the number of data, this criterion is not strictly convex, i.e. the solution cannot be a-priori guaranteed to be unique. In practice, minimizing this L1-norm penalized LS fitting criterion is much easier than minimizing the original one based on the L0-norm, and many computationally efficient algorithms have been developed, some of which can be made compatible with a real-time system using a 1kHz clock-time. However, minimizing eq.(A3b) does not necessarily lead to the same solution than minimizing eq.(A3a). Theoretical conditions guaranteeing the equivalence of both solutions have been established, which are based on properties of the matrix **W**, so depend on the specificities of the problem being considered.

The choice of the family of atoms is critical in the Sparse Representations of signals as, with an appropriate choice, these atoms might be well adapted to the signal to be analyzed and might lead to a matrix **W** with good analytical and numerical properties. For example, it can be shown that if the signal can be represented with $\|\mathbf{x}\|<(1+1/m)/2$ components, with $m = \max_{k\neq l}(|\mathbf{w}_k^H \mathbf{w}_l|)$, where $\mathbf{W}^H$ is the Hermitian transposition of **W,** then minimizing eq.(3b) will lead to select the same atoms than the solution minimizing eq.(A3a) [37]. For these reasons, the matrix **W** is often chosen as a union of incoherent basis, such as wavelets, Diracs, pure sine waves, or other mathematical approaches.

In our case, the atoms are imposed by the model setup in eq.(A2) to be pure complex exponential waves, $\mathbf{W} = \{\exp(i n_k \phi_p)\}_{p,k}$, for $p = \{1, \ldots, P\}$ and $k = \{1, \ldots, M\}$, with $n_k = k-K+1$ and $M = 2K+1$. Due to the irregular sampling, the atoms are strongly correlated. Indeed, it can be shown that $|w_k^H w_l| = \hat{W}(n_k - n_l)$, so that it corresponds to regular samples of the spectral window. As ($\hat{W}(\nu)$ may take values greater than 1/3 (as shown in figA1), the previous condition guarantees exact detection only if the signal consists of a single mode number. Nevertheless, it has been shown from many simulations and analysis of measurements using comparison between different numerical methods that such a solution generally gives very satisfactory results in terms of detection, even in the case of multiple modes. Moreover, for irregular sampling, uniqueness of the global minimizer is almost surely guaranteed if it has less than P/2 non-zero components, where P is the data size [12].

In terms of amplitude estimations, it has been shown [11, 12] that minimizing eq.(A3b) leads to an under-estimation of the amplitudes of the detected mode numbers due to the L1-norm penalization term of eq.(A3b). Thus, an a-posteriori LS estimation of these amplitudes can be (and usually is for post-pulse analysis) performed in a second step within the calculations, after the modes are actually detected. The amplitudes of the detected modes are computed, minimizing the least square criterion $\|\mathbf{y}-\mathbf{W}_{DET}\mathbf{x}_{DET}\|^2$ where only the non-zero amplitudes of the optimization step are preserved in $\mathbf{x}_{DET}$. Note that this a-posteriori amplitude estimation step is not an absolute necessity for the real-time analysis, as its main objective is to detect the actual modes, their mode numbers and frequency width, and not to precisely estimate their absolute amplitudes, a scaled value being sufficient for these purpose. A real-time implementation of the proposed modes detection method requires not only an efficient optimization algorithm to minimize eq.(A3b) but also, even more importantly for a frequency-degenerated spectrum, an efficient unsupervised tuning of the penalization parameter λ. Many numerical algorithms are available to minimize criteria such as those of eq.(A3b) for Sparse Approximations. While for real-valued unknowns $\mathbf{x}_k$ this problem can be written as a classical Quadratic Program, for complex-valued unknowns $\mathbf{x}_k$ it corresponds to a Second-Order Cone Program [38]. An algorithm based on an iterative Block Coordinate Descent procedure has been previously proposed [11, 12], and implemented in the *SparSpec* code. This procedure consists of performing successive one-dimensional minimization steps with respect to each complex-valued unknown $\mathbf{x}_k$, where each one-dimensional minimization has an explicit solution. This algorithm is very efficient and a correct solution can be typically found in less than 1ms using the rather modest computational resources available to process real-time JET data.

The penalization parameter l is related to the noise level and requires an appropriate tuning, since it increases the penalty for those solutions which invoke a large number of modes. It can be shown that for $\lambda > \lambda_{MAX} = \max(|W^H y| = \max_k(|\hat{y}(n_k)|)$, the minimizer $\mathbf{x}_{MIN}$ of eq.(A3b) is identically zero, i.e. the unique solution has no detected modes; and (b) for a given λ, the minimizer $\mathbf{x}_{MIN}$ of eq.(A3b) satisfies $\max(|W^H(y - Wx_{MIN})|) = \max_k(|\hat{r}(n_k)|) \leq \lambda$, where

$\mathbf{r} = \mathbf{y} - \mathbf{W}\mathbf{x}_{\mathbf{MIN}}$ is called the residual (data minus the model corresponding to the estimated modes). Hence λ can be interpreted as the maximum peak amplitude allowed in the periodogram of the residual, and choosing λ to be a fraction $\lambda_{NORM} \in [0, 1]$ of the maximum of the periodogram of the data $\lambda = \lambda_{NORM} \times \max(|\mathbf{W}^H\mathbf{y}|)$, ensures the periodogram of the residual $\mathbf{r}$ to be lower up to this fraction relatively to the maximum of the data periodogram. Hence knowledge of the noise level in the measurements helps to determine the optimum value for λ_{NORM} to be used for real-time and post-pulse analysis of MHD fluctuation data. For real-time MHD analysis at JET, the most suitable value for λ_{NORM} was determined to be $\lambda_{NORM} = 0.85$ as this value allows for a very rapid convergence of the optimization algorithm and is sufficient to detect and discriminate multiple modes whose amplitudes are of interest for MHD diagnostic purposes.

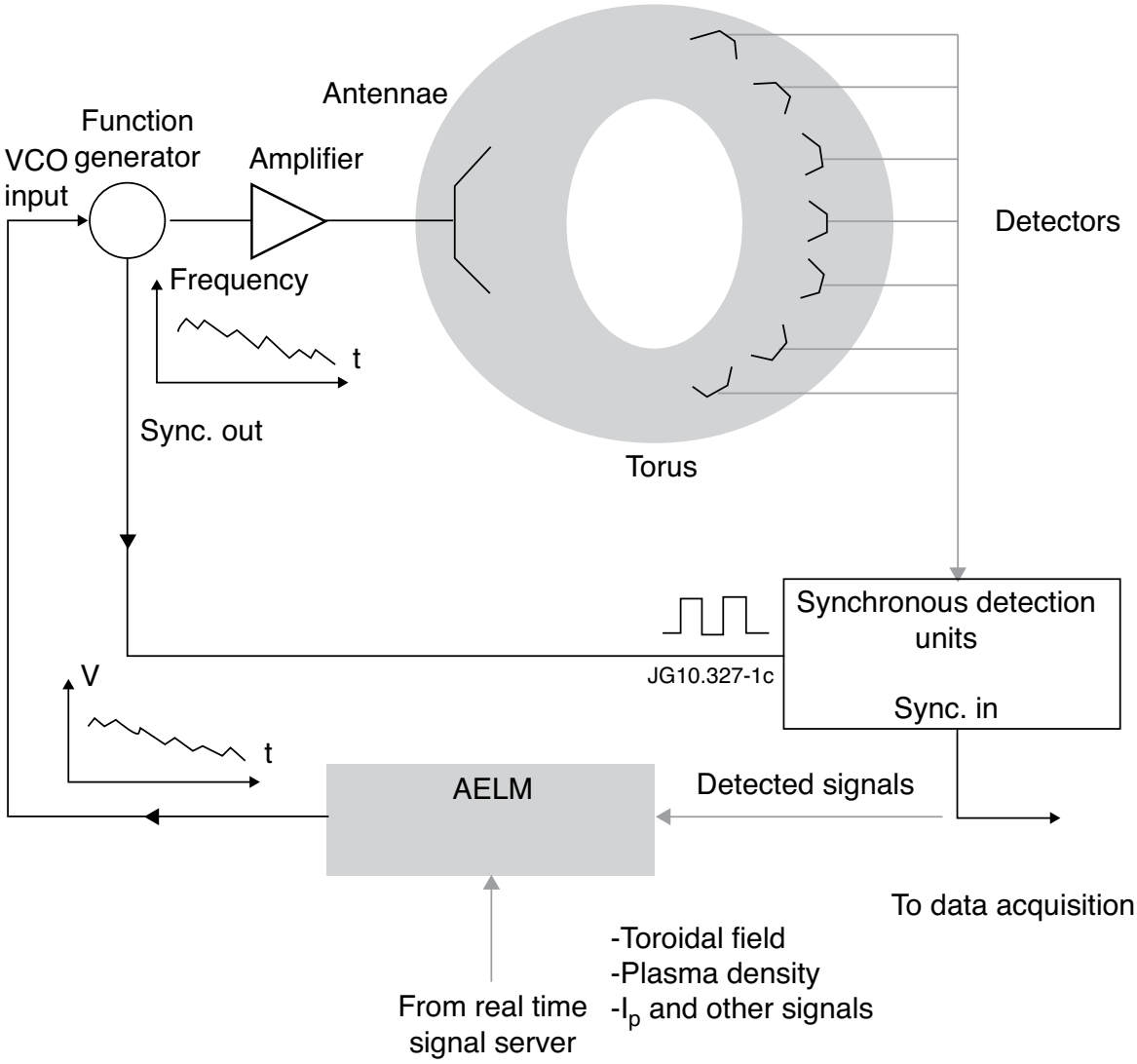

Figure 1: A schematic overview of the AEAD system in JET. The toroidal field, plasma density and plasma current (I_p) are required to compute in real-time an initial guess for the frequency of Alfvén Eigenmodes. This value is then converted as a time-dependent voltage V(t) and is sent as a Voltage Controlled Oscillator (VCO) input signal to the function generator which, in turn, converts it back into a frequency freq(t). This signal then drives a high-power amplifier connected to in-vessel antennas and the synchronous detection units via an optical transducer, so that only the portion of the plasma response which has the same frequency of the antenna drive (i.e. it is synchronous with them) is detected in real-time, which avoids the need for computationally expensive FFT algorithms.

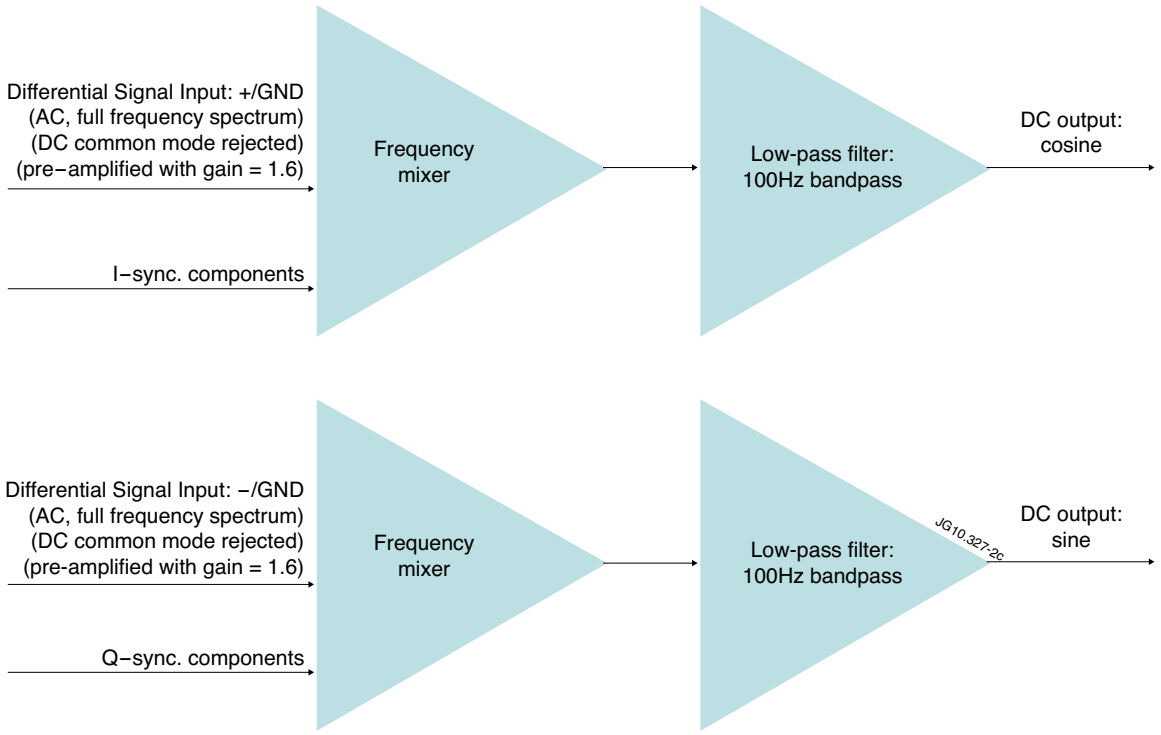

Figure 2: A schematic diagram illustrating the AEAD synchronous detection hardware. This hardware is conceptually based upon first removing any DC common mode from the input AC differential signal (with a full frequency spectrum), which is then amplified, and then applying a low-pass filter to extract only the component in the input signal which is at the desired (i.e. synchronous) frequency

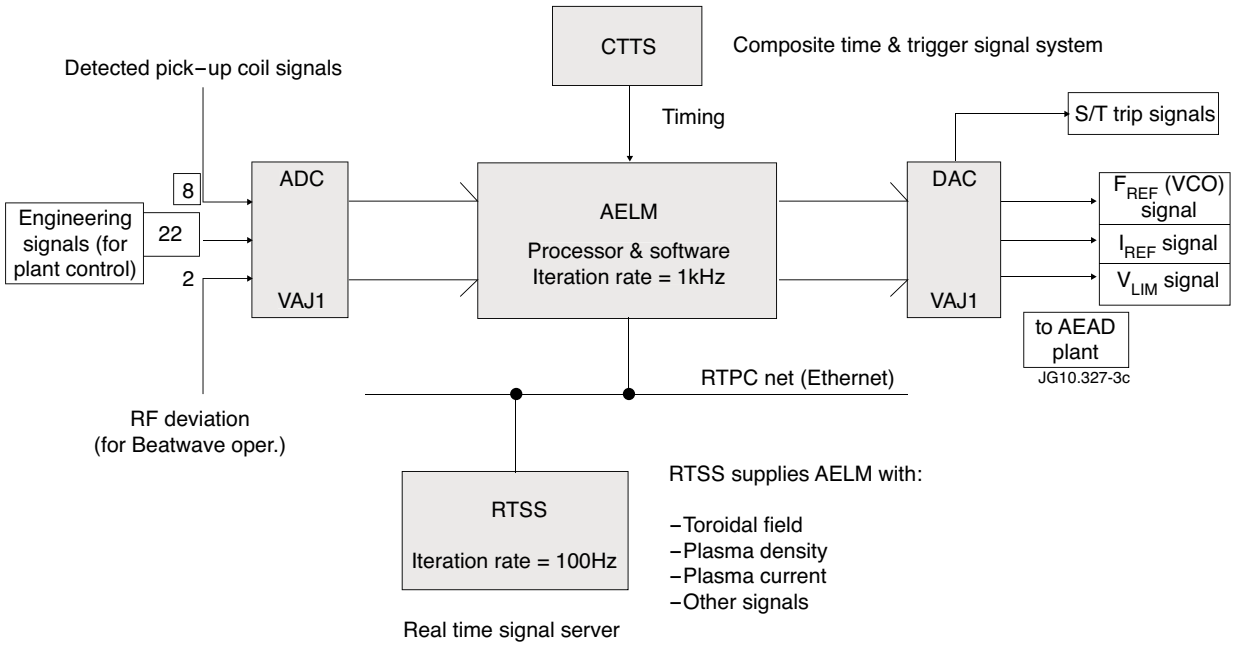

Figure 3: A schematic diagram of the AELM hardware, illustrating its interfaces with the Real Time Signal Server (RTSS) and the Central Time and Trigger Signal System (CTSS), which monitor and control in real-time the overall operation of the JET tokamak, and the input and output connections to the AEAD plant via the VAJ1 cards and the Ion Cyclotron Resonance Frequency (ICRF) heating system for real-time control of the RF beatwave operation.

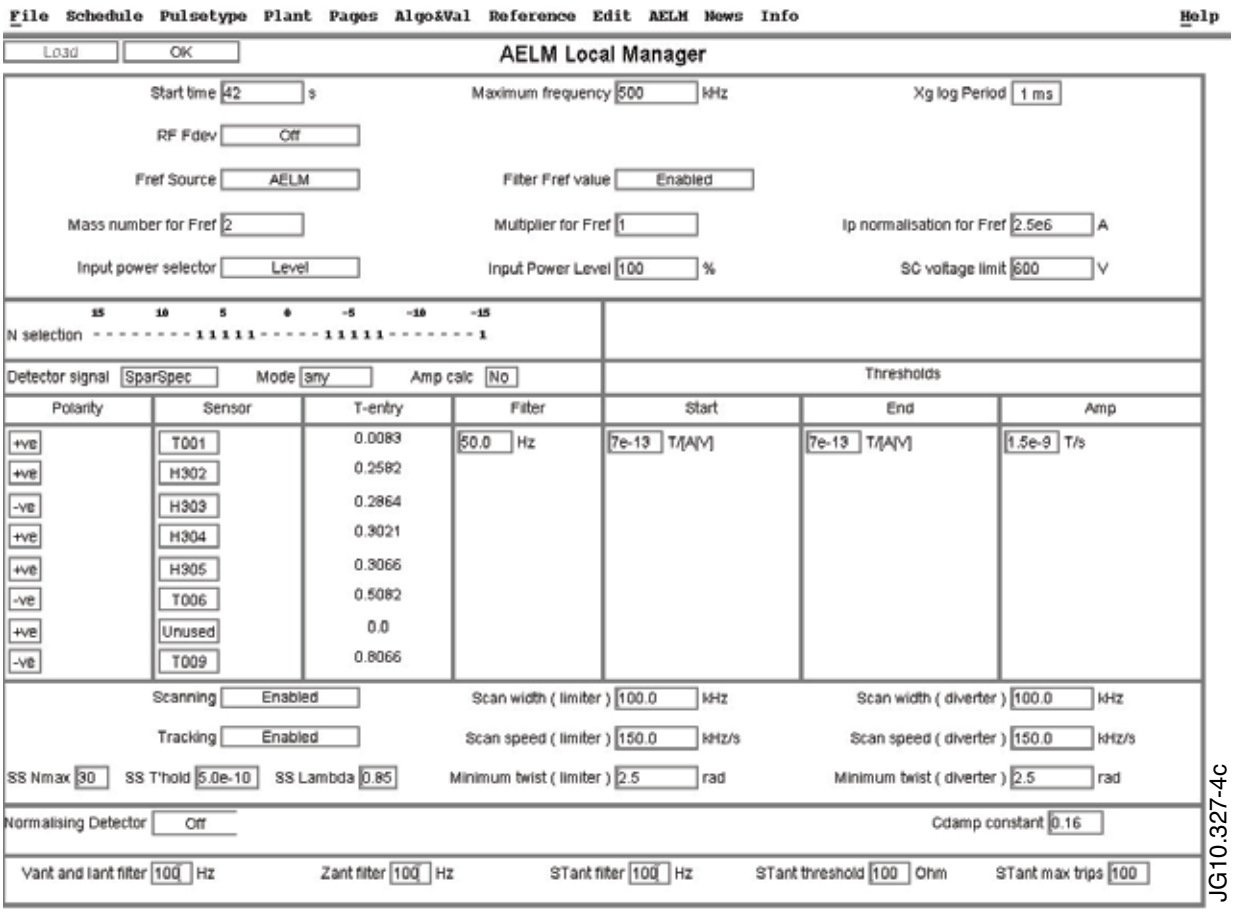

Figure 4: The AELM configuration panel, shown here for the SparSpec algorithm and frequency control via the real-time TAE frequency.

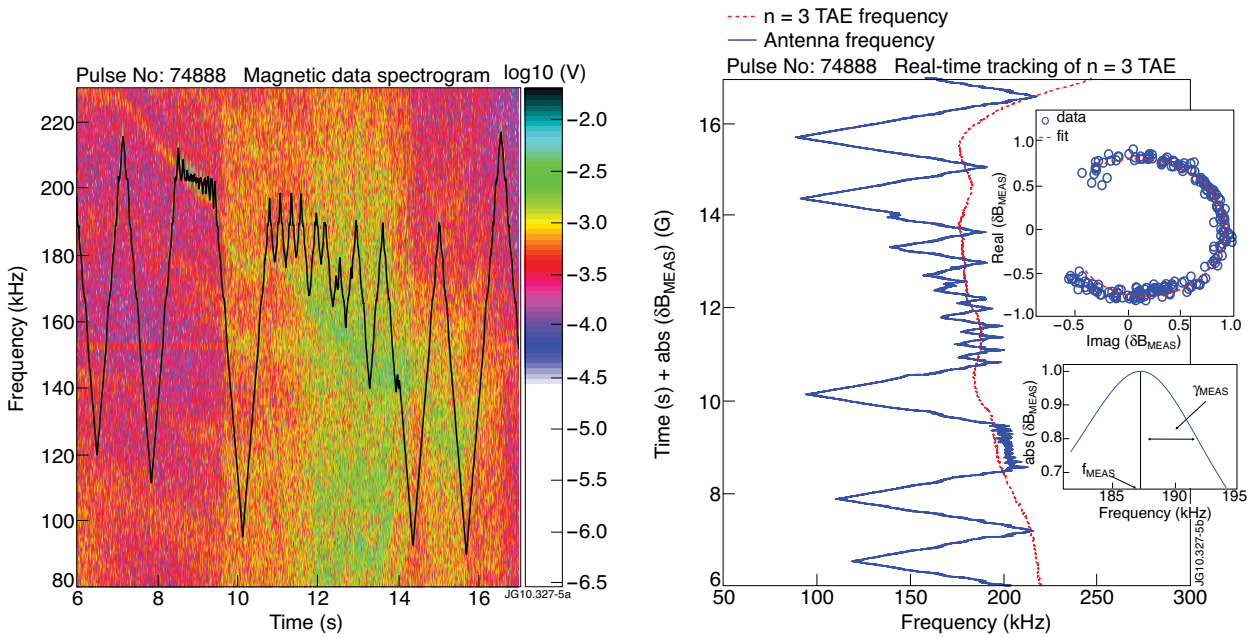

Figure 5: An example of the real-time tracking of an n = 3 TAE for the JET Pulse No: 74888.

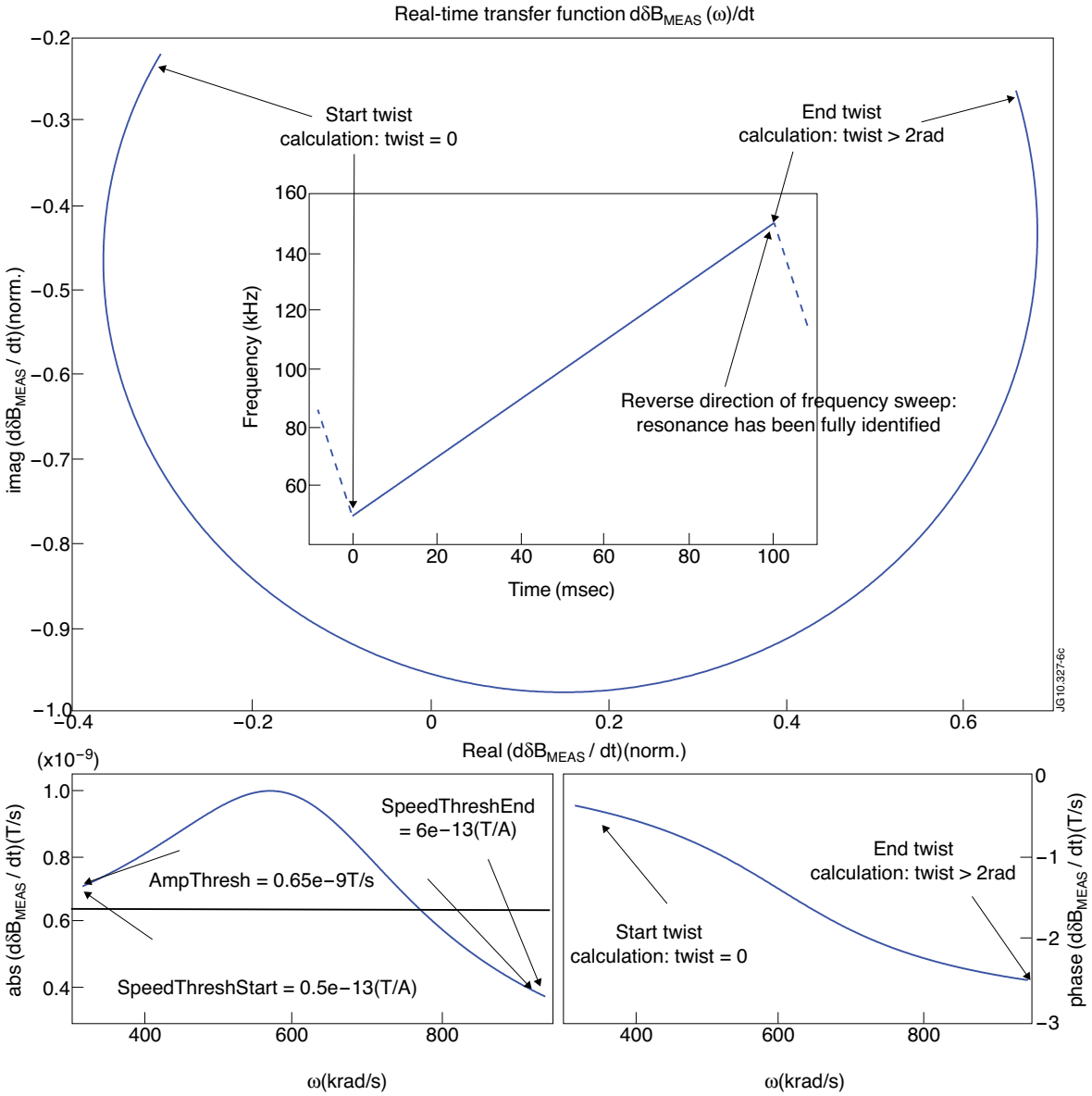

Figure 6: A schematic diagram to illustrate the basic ideas of the real-time tracking algorithm.

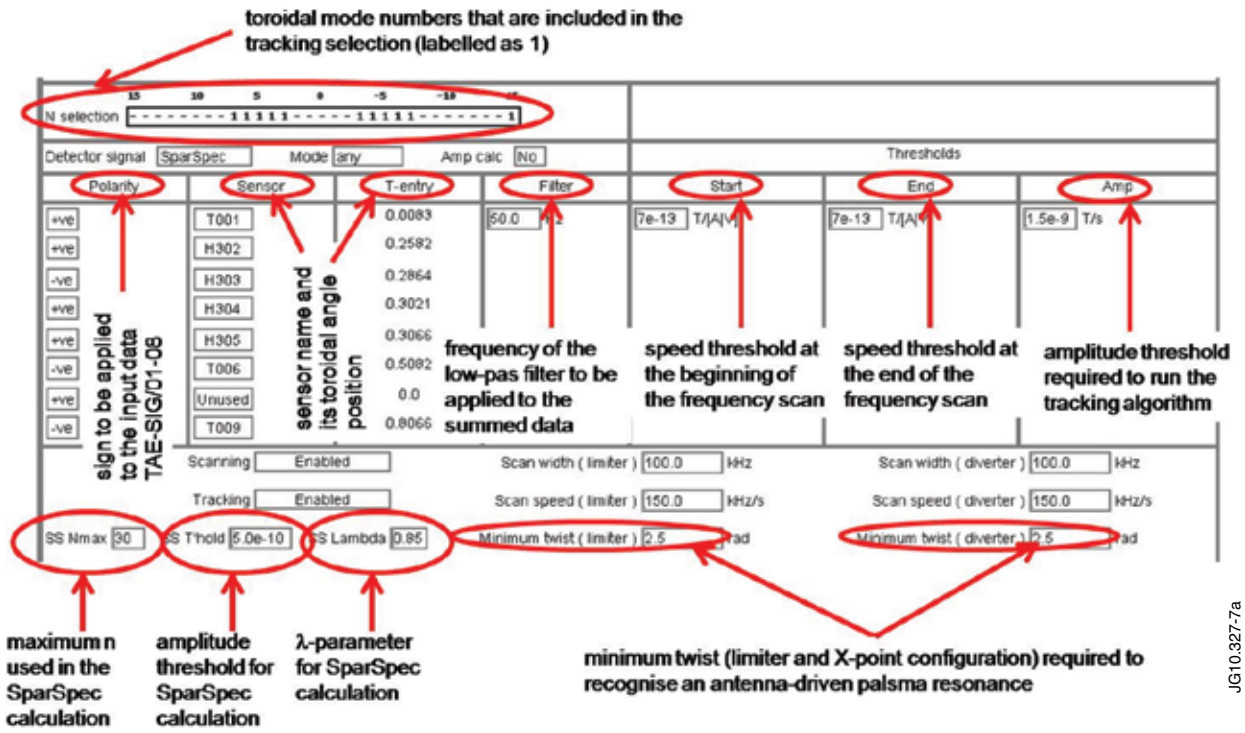

Figure 7(a): Setting up the mode detection parameters for the SimpleSum algorithm.

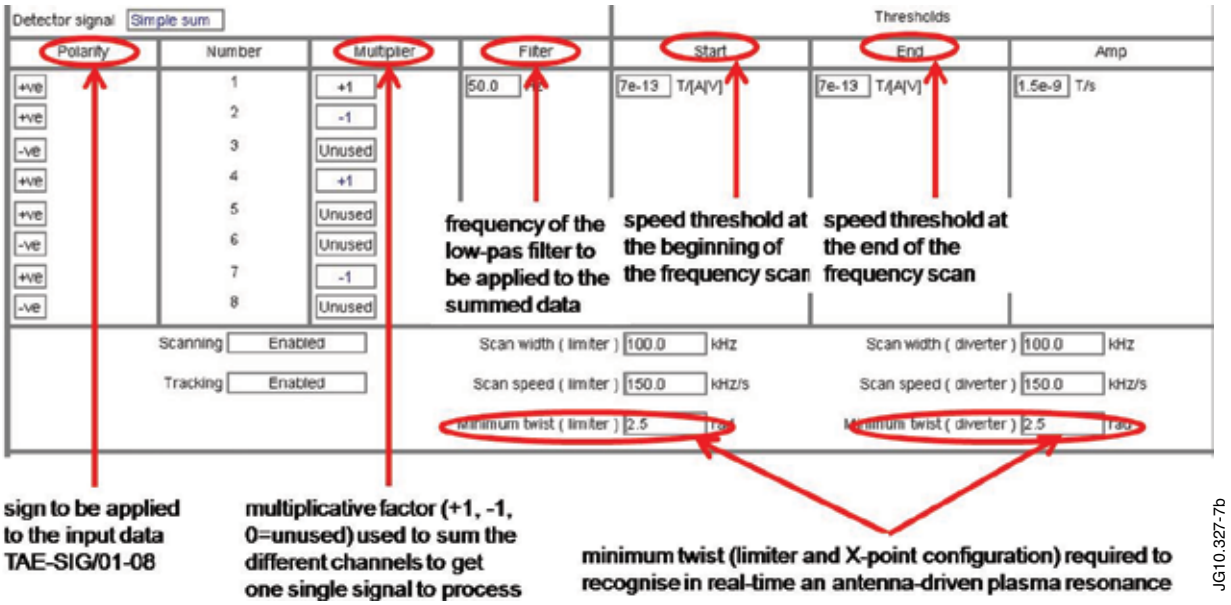

Figure 7(b): Setting up the mode detection parameters for the SparSpec algorithm: the "any" mode of operation is shown, but the parameters are the same when using the "highest" mode of operation.

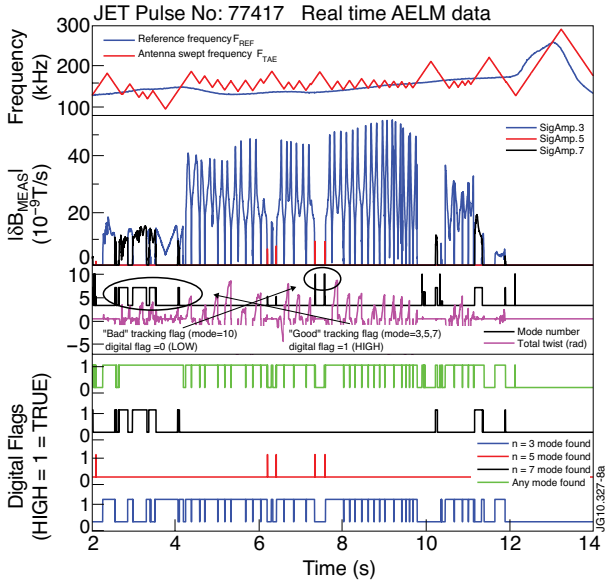

Figure 8 (a): An example of real-time tracking of the individual n = [3, 5, 7] TAEs for the JET Pulse No: 77417; the signal SigAmp.N shows the amplitude of the n = N modes as detected in real-time; the n = 10 mode corresponds to bad tracking because its digital validity flag is false (= 0).

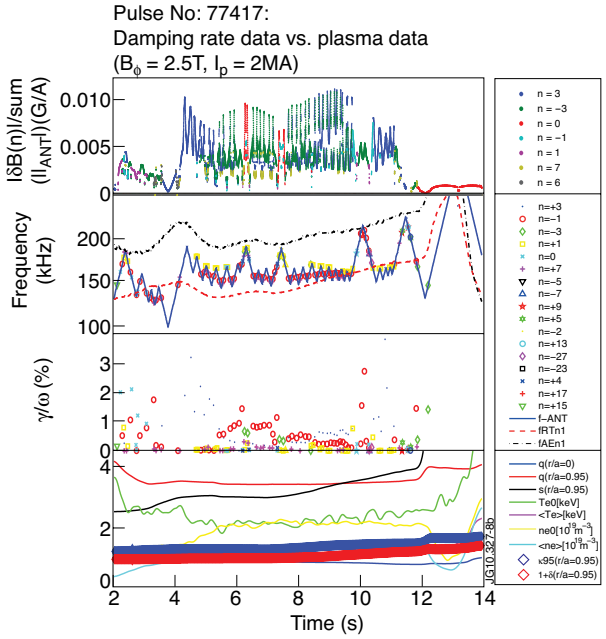

Figure 8 (b): Post-pulse analysis of the AEAD data for Pulse No: 77417; the quantity F(n = 1, x = 0) shows the value of the mode frequency as calculated at the centre of the n = 1 TAE gap using the equilibrium magnetic configuration and the measured density and safety factor profiles.

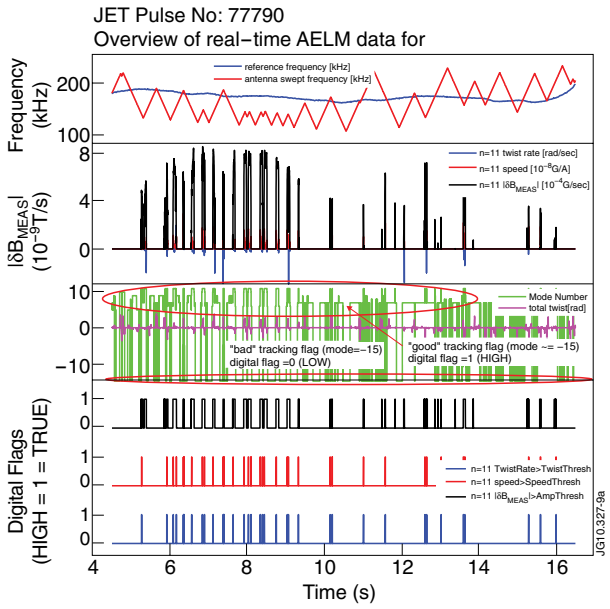

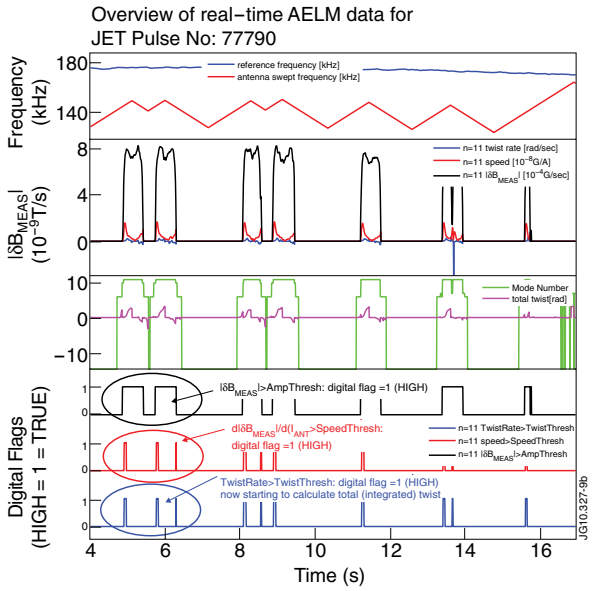

Figure 9: (a,b). A real-time example of the twist and speed calculations for the JET Pulse No: 7790 and the n=11 TAE mode (fig.9a, left frame); the zoom shown in fig9b (right frame) demonstrates that the tracking of the n=11 mode only occurs when all the resonance conditions are above the set thresholds, i.e. the digital flags for the mode amplitude and speed are concurrently high (see the bottom frame).

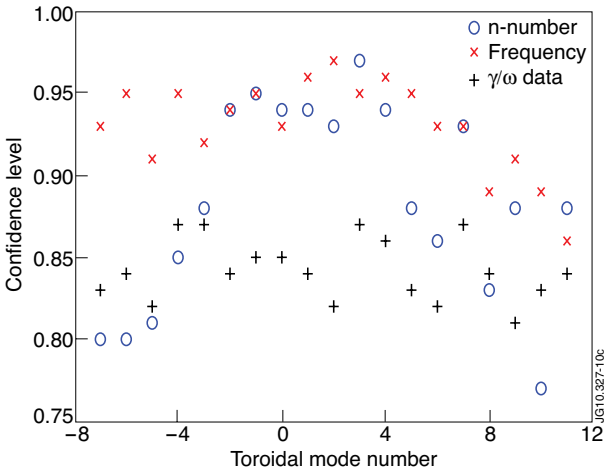

Figure 10: Confidence level for the real-time evaluation of the mode number, frequency and damping rate when using the SparSpec tracking algorithm.

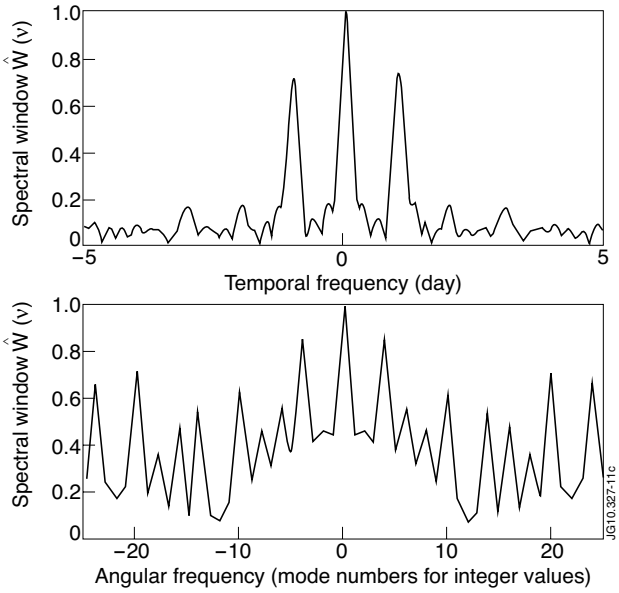

Figure A1. The spectral windows corresponding to an example of astronomical observations during five nights (top) and to the actual positions of the seven magnetic sensors that are sufficiently reliable to be used in the real-time data processing algorithm for the analysis of MHD instabilities (bottom) in JET.